

Non-universal Scaling of Thermoelectric Efficiency in 3D and 2D Thermoelectric Semiconductors

Kevin Octavian^{1,a)}, Eddwi H. Hasdeo^{2,3,b)}

¹Engineering Physics, Faculty of Industrial Technology, Institut Teknologi Bandung, Indonesia

²Research Center for Physics, Indonesian Institute of Sciences, South Tangerang, Indonesia

³Department of Physics and Material Science, University of Luxembourg, Luxembourg

E-mail: ^{a)}kevin.octavian@itb.ac.id

^{b)}eddw001@lipi.go.id

Abstract. We performed the first-principles calculation on common thermoelectric semiconductors Bi₂Te₃, Bi₂Se₃, SiGe, and PbTe in bulk three-dimension (3D) and two-dimension (2D). We found that miniaturization of materials does not generally increase the thermoelectric figure of merit (ZT) according to the Hicks and Dresselhaus (HD) theory. For example, ZT values of 2D PbTe (0.32) and 2D SiGe (0.04) are smaller than their 3D counterparts (0.49 and 0.09, respectively). Meanwhile, the ZT values of 2D Bi₂Te₃ (0.57) and 2D Bi₂Se₃ (0.43) are larger than the bulks (0.54 and 0.18, respectively), which agree with HD theory. The HD theory breakdown occurs because the band gap and band flatness of the materials change upon dimensional reduction. We found that flat bands give a larger electrical conductivity (σ) and electronic thermal conductivity (κ_{el}) in 3D materials, and smaller values in 2D materials. In all cases, maximum ZT values increase proportionally with the band gap and saturate for the band gap above $10 k_B T$. The 2D Bi₂Te₃ and Bi₂Se₃ obtain a higher ZT due to the flat corrugated bands and narrow peaks in their DOS. Meanwhile, the 2D PbTe violates HD theory due to the flatter bands it exhibits, while 2D SiGe possesses a small gap Dirac-cone band.

1. Introduction

Thermoelectric (TE) materials are useful for generating electricity from waste heat without any moving parts. Despite decades of research in this field, TE efficiency remains low and stagnant at 10%. This efficiency corresponds to a dimensionless figure of merit (ZT) that equals to unity, which is defined as

$$ZT = \frac{S^2 \sigma}{\kappa_{el} + \kappa_{ph}} T, \quad (1)$$

where S is the Seebeck coefficient, σ is the electric conductivity, κ_{el} is the electronic thermal conductivity, κ_{ph} is the phonon thermal conductivity, and T is the effective

temperature. High electric conductivity is needed to obtain a high ZT value, but increasing it also increases the thermal conductivity, following the Wiedemann-Franz law $\kappa_{el} = \sigma L T$, where L is the Lorenz number. This proportionality reduces ZT value. It is hard to achieve a ZT value over unity due to this relation.

Another factor that reduces the ZT further is the fact that metals exhibit a low Seebeck coefficient, while insulators have the opposite characteristics. Thus good TE materials usually come from semiconductor materials. There exists a range of band gaps [1, 2] and band widths [3] which give the optimal ZT

value.

One way to push ZT value beyond unity is through the miniaturization of materials as initially proposed by Hicks and Dresselhaus (HD) [4, 5]. The density of states in 2D and 1D materials show sharp steps and the Van Hove singularities, respectively, which are responsible for the increase of the Seebeck coefficient and hence the ZT value as well. The breakthrough of ZT values has been observed in 1D and 2D nanostructured materials, such as hierarchical PbTe [6], silicon nanowires [7], nanostructured BiSbTe [8]. However, the enhancement due to miniaturization of materials only works when the confinement length is smaller than its thermal de Broglie wavelength [9]. With recent advances in crystal growing of 2D materials, it is possible to have one or few atoms-thick 2D materials that satisfy small confinement lengths.

Moreover, HD theory simply assumes parabolic bands that retain the same band gaps and band flatness as the dimension changes. In reality, these quantities strongly depend on the geometry and the dimension of the materials, and as a result, they will affect TE transport. In this paper, we investigate several common semiconductors TE to check the limitation of the HD theory.

We investigate the 3D and the 2D structures of Bi₂Te₃, Bi₂Se₃, PbTe and SiGe. The TE properties were calculated by using the first-principles calculation and the Boltzmann transport equation. Additionally, these results can be compared with a simple two-band model to understand the dependence of TE properties on dimensionality, band gap, and band flatness. While the bulk states of these materials are considered as good TE materials, the TE properties of the 2D structures remain in early-stage research. The single quintuple layer (QL) of Bi₂Te₃ and Bi₂Se₃ have been experimentally fabricated through exfoliation [10, 11]. In the recent study [12], it has been shown that the (001) PbTe monolayer turns into a 2D topological crystalline insulator while SiGe has a graphene-like structure on its 2D surface (siligene) [13].

Our results show that dimension reduction changes the band gaps and the flatness of the band. From the analysis of the two-band model, we show that the band flatness keeps the Seebeck coefficient intact and reduces the σ and κ_{el} values in 2D materials, while in 3D materials, it increases σ and κ_{el} due to the different density of states. Overall, the maximum ZT values increase proportionally with band gap and saturate when band gap above $10 k_B T$ in both the 2D and 3D materials. As a result, 2D PbTe, which exhibits relatively flat bands, and 2D SiGe, which has a low band gap, have a low ZT value, and violate HD theory. On the other hand, Bi₂Te₃ and Bi₂Se₃ agrees with HD theory because of their flat corrugated bands [14] and a lot of narrow peaks on the DOS giving an enhancement in their ZT values. Our results also show that the ZT values of the investigated materials increase as the temperature increase, except for Bi₂Te₃.

2. Methods

We used Quantum Espresso [15] to perform all density functional theory (DFT) calculations with the projected augmented wave (PAW) method [16]. The generalized-gradient approximation (GGA) of Perdew-Burke-Ernzerhof (PBE) functional was used as the exchange-correlation [17]. The plane wave's cutoff energy and the charge density were set to 60 Ry and 720 Ry, respectively. The Monkhorst-Pack scheme [18] was used to integrate the Brillouin zone in the self-consistent calculations with a k-point mesh of $10 \times 10 \times 10$ for the bulk materials and $10 \times 10 \times 1$ for the 2D materials. A vacuum layer of 35 Å is used for the 2D calculations. The convergence criteria

Table 1. Fitted relaxation times and phonon thermal conductivities at 300K

Material	τ (10^{-14} s)	κ_{ph} (W/mK)
Bi ₂ Te ₃	2.8	1.37
Bi ₂ Se ₃	0.7	1.00
PbTe	1.1	2.15
SiGe	0.8	4.60

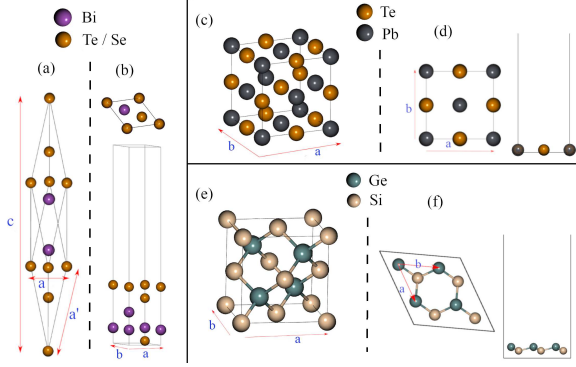


Fig. 1. Crystal structures of (a) bulk Bi_2Te_3 or Bi_2Se_3 , (b) a single QL of Bi_2Te_3 and Bi_2Se_3 , (c) bulk PbTe , (d) $\text{PbTe}(001)$ monolayer, (e) bulk SiGe , and (f) $\text{SiGe}(001)$ monolayer

for structure optimization was taken to be less than 10^{-3} eV and less than 0.025 eV \AA^{-1} for the total energy and the total force, respectively.

The semi-classical Boltzmann equations encoded in the BoltzTraP program was used to evaluate the transport properties [19]. To give a better result, a denser k-mesh of $40 \times 40 \times 40$ and $80 \times 80 \times 1$ were used for the bulk materials and the 2D materials, respectively. Relaxation time (τ) and phonon thermal conductivity (κ_{ph}) were required to evaluate the dimensionless figure of merit (ZT) of a material. The values presented in Table 1 are obtained by using the method described in Appendix A of Supplementary Material [20] for all bulk materials. We employed the same values to the corresponding 2D materials.

3. Results and Discussion

3.1. Structural Properties

The phase groups of the materials that we used are as follow, $R\bar{3}m$ for Bi_2Te_3 and Bi_2Se_3 , $Fm\bar{3}m$ for PbTe , and $F\bar{4}3m$ for SiGe . As for the 2-dimensional structures, the quintuple layer (QL) of Bi_2Te_3 and Bi_2Se_3 , and (001) surface layer of PbTe and SiGe were used. In this study we only investigated a single layer of each materials. All of the structures are presented in Fig. 1.

The results of our structure optimization are shown in Table. 3 of Supplementary Material. The error between our results and the experiment values are less than 2 %. A further reduction in error could be obtained by using tighter convergence criteria. Bulk Bi_2Te_3 and Bi_2Se_3 both have the same hexagonal close-packed (HCP) crystal structure. Bulk PbTe has a NaCl face-centered cubic crystal structure. The surface of PbTe in (001) direction possesses a similar lattice constant with the bulk structure, although it is stated in [21] that the lattice constant of (001) few-layers decreases drastically, but the magnitude is unclear for the monolayer PbTe . The (001) surface of SiGe (siligene) has a similar structure with graphene. Nevertheless, unlike planar graphene, siligene possesses a buckling structure. The calculated buckling amplitude is 0.58 \AA , which agrees with the previous theoretical work [22].

3.2. Electronic Structure

The calculated electronic band structures of each material are shown in Fig. 2. All bulk materials except SiGe have direct band gaps, while for the 2D counterparts, only PbTe and SiGe have the direct band gaps. The siligene exhibits a Dirac cone-shaped band structure at the K point, which was previously found in [13] and [22]. Bi_2Te_3 and Bi_2Se_3 possess a similar band structure due to their similarity in structure. The band structure of both materials in bulk has a direct band gap at Γ -point, while the inclusion of spin-orbit coupling (SOC) causes a band inversion [23]. As for the single QL, the band structure of Bi_2Te_3 without the inclusion of SOC is similar to the previous theoretical calculation [24], where SOC was included.

The band gap values of each material are presented in Table 2. Comparing with the references, we can see that the inclusion of SOC reduces the conduction band energy, especially in materials consisting of heavy atoms. The band energy reduction results in the lowering of the band gap and band inversion in some cases, like Bi_2Te_3 . SOC does

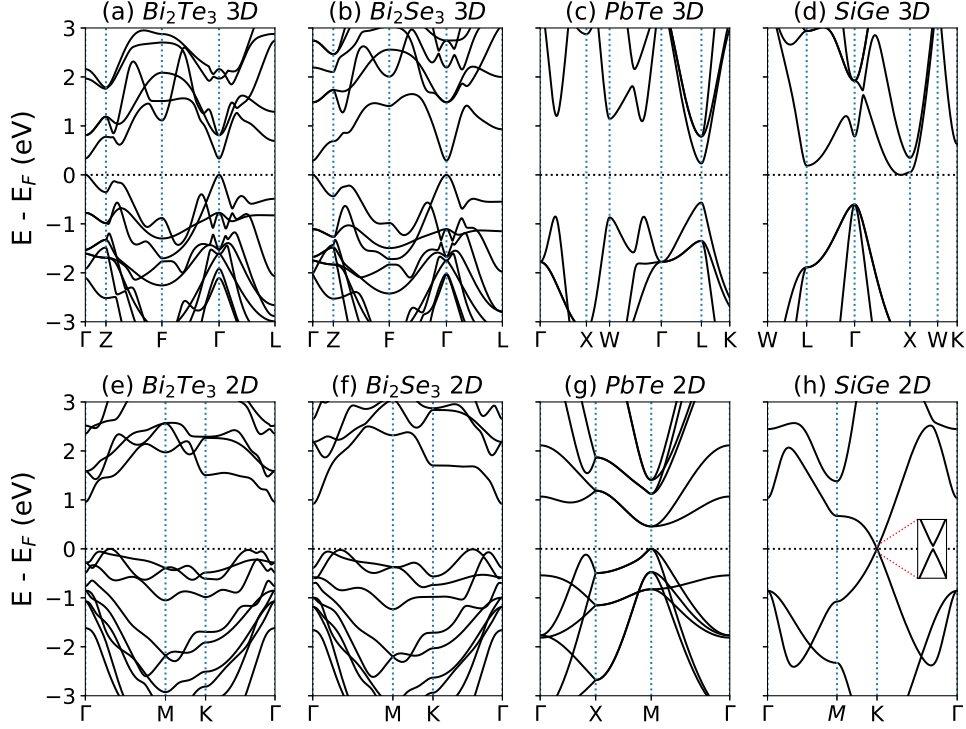


Fig. 2. The calculated band structure of (a) bulk Bi_2Te_3 , (b) bulk Bi_2Se_3 , (c) bulk PbTe , (d) bulk SiGe , (e) single QL of Bi_2Te_3 , (f) single QL of Bi_2Se_3 , (g) PbTe monolayer, and (h) SiGe monolayer

Table. 2. The calculated band gap of each material

	This Work (eV) (Without SOC)	Previous Work (eV) (With SOC except SiGe)
3D Material		
Bi_2Te_3	0.33	0.11 [25]
Bi_2Se_3	0.28	0.26 [26]
PbTe	0.79	0.19 [27]
SiGe	0.6	1.018 [28]
2D Material		
Bi_2Te_3	0.94	0.32 [24]
Bi_2Se_3	0.91	-
PbTe	0.45	0.11 [21]
SiGe	0.0052	0.012 [22]

not affect SiGe tremendously because SiGe is composed of light atoms. We note that the GGA underestimates the semiconductor band gaps, which raises a discrepancy between this work and the reference that uses the GGA+U method. The total density of states (DOS) for all materials are shown in Fig. 3. The energy

is shifted to the valence band maximum to set it as the reference. In all cases, the DOS near the valence band edge is larger and denser for the 2D structures than the bulk.

3.3. Thermoelectric Properties

The calculated Seebeck coefficients as a function of chemical potential at 300 K are shown in Fig. 4. This study focuses only on longitudinal transports to compare the bulk with the two-dimensional properties. The properties of all materials are isotropic. The chemical potential is related to the carrier concentration. Increasing the chemical potential or carrier concentration way above the gap will decrease the Seebeck coefficient.

The single QL of Bi_2Te_3 and Bi_2Se_3 have a higher Seebeck coefficient compared to the bulk properties. On the contrary, the bulk properties of SiGe and PbTe have a much higher Seebeck coefficient than the 2D

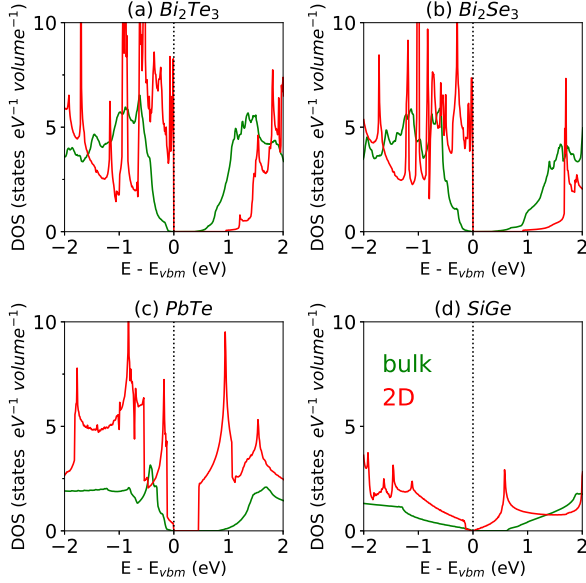


Fig. 3. Density of States (DOS) of (a) Bi_2Te_3 , (b) Bi_2Se_3 , (c) SiGe , and (d) PbTe . The green colour represents the DOS of the bulk structures and the red represents the 2D structures.

counterparts. Single QL of Bi_2Te_3 achieved the highest Seebeck coefficient for the 2D materials and PbTe exhibits the highest Seebeck coefficient for the 3D materials, with a value of $1610 \mu\text{V/K}$ and $1375 \mu\text{V/K}$ respectively.

The second row of Fig. 4 shows the calculated electrical conductivity as a function of chemical potential at 300K. Unlike the Seebeck coefficient, increasing the chemical potential results in the increase of electrical conductivity. P-type Bi_2Te_3 has the highest bulk electrical conductivity ($\sim 24 \times 10^6 \text{ S/m}$) while n-type PbTe has the highest conductivity among the 2D materials ($\sim 3 \times 10^6 \text{ S/m}$). Bi_2Se_3 has the smallest magnitude of electrical conductivity. Overall, the electrical conductivities of the 2D structures are lower compared to their bulk structures.

The calculated electronic thermal conductivities are shown in the third row of Fig. 4. Comparing with electrical conductivity, the thermal conductivity of each material has sim-

ilar trends. From the second and third row, we can see that the increase of electrical conductivity also increases electronic thermal conductivity, which aligns with the Wiedemann-Franz law.

The ZT values are shown in the last row of Fig. 4. We can see that SiGe has the lowest maximum ZT values, which are around 0.09 for the n-type bulk SiGe and 0.04 for the p-type 2D SiGe . The low ZT value in bulk SiGe is due to the high phonon thermal conductivity that it exhibits. The single QL of Bi_2Se_3 and Bi_2Te_3 achieves a higher maximum ZT value than the bulk structure. The highest ZT value is achieved by p-type Bi_2Te_3 on its bulk (~ 0.54) and 2D structure (~ 0.57). The 2D materials do not necessarily improve the ZT value. Bi_2Se_3 and Bi_2Te_3 get the ZT enhancement due to the enhancement in their Seebeck coefficients, while there are materials with lower ZT values than its bulk structure such as SiGe and PbTe .

The band flatness and the band gap are changed upon dimensional reduction, as seen in Fig. 2. To investigate the effects they have on transport properties, we calculate the transport properties using a two-band model, with a Kane band as the conduction band and a parabolic band as the valence band to emulate the asymmetrical bands near the Fermi level. The formulation can be seen in Appendix B of Supplementary Material, and the results are shown in Fig. 5, Fig. 6 and Fig. 10 - 12 in Supplementary Material.

From this simple model, we can see that band flatness gives a positive enhancement to the TE properties in 3D material while it has a detrimental effect on 2D material. Changing the band flatness will only affect the Kane band in CB, thus we only plot ZT_{max} vs band gap $\tilde{\Delta}$ for n-doped only (Fig. 6). Band flatness does not affect the Seebeck coefficient significantly, but rather it affects σ and κ_{el} more (Fig. 10 - 12). In 2D systems, σ and κ_{el} decrease as the band becomes flatter while the Seebeck coefficient remains the same. As a result, the ZT in 2D materials possessing a flat band is lower than those with

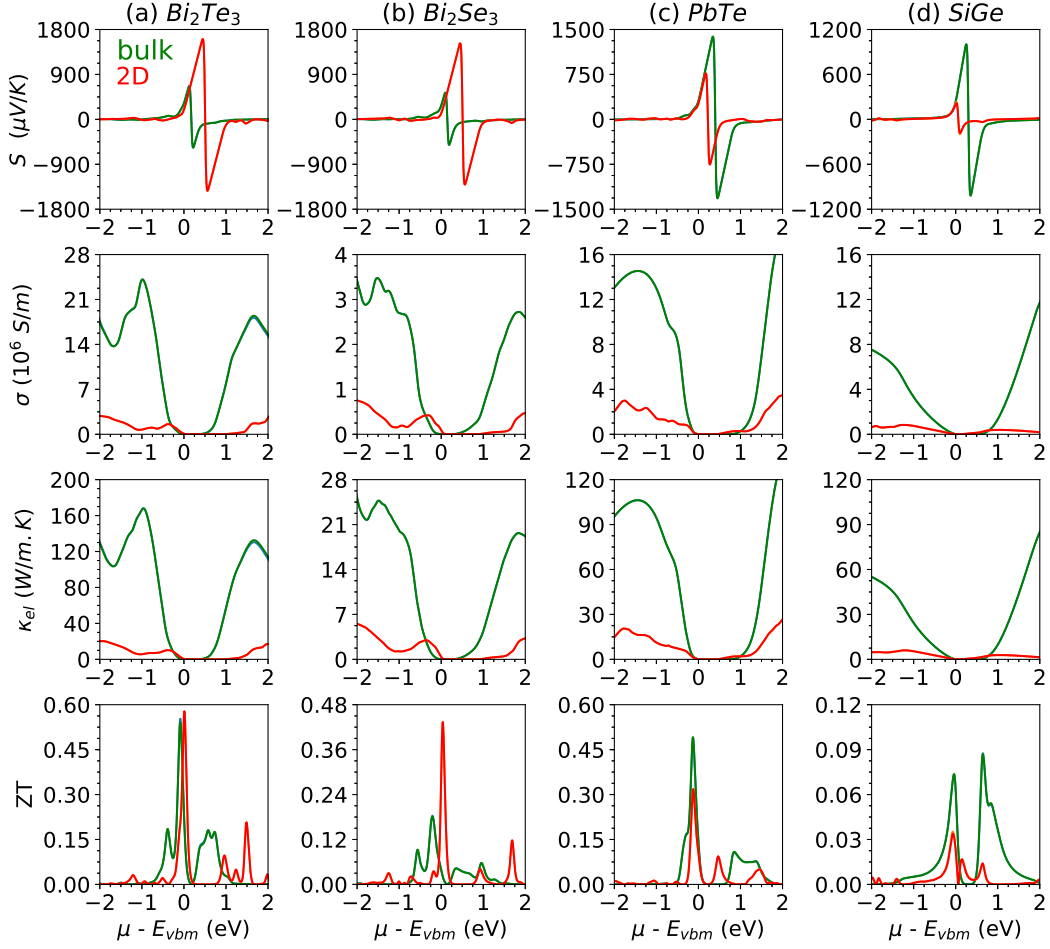


Fig. 4. Thermoelectric Properties for (a) Bi_2Te_3 , (b) Bi_2Se_3 , (c) PbTe , (d) SiGe . The properties from the first row to the last: Seebeck Coefficient, Electric Conductivity, Electronic Thermal Conductivity, and ZT Values. Bulk and 2D properties are indicated by the green line and red line respectively.

a more dispersive band. On the contrary, band flatness has the opposite effect on TE properties in 3D due to different DOS. Aside from band flatness, the asymmetrical effective mass parameter described in Ref. [29] might affect TE properties. However, in this work, we assume the masses to be the same. This ratio only affects the 3D systems and has no effects on the 2D, because there is no mass terms in the 2D TE integral (Eq. 18-21 of Supplemental Material).

In general, the maximum ZT value (ZT_{max}) increases proportionally with the band gap in both the 3D and 2D materials.

The maximum ZT values increase as the band gap widens up to a certain threshold value, which is around $10k_B T$ or 0.25 eV at room temperature, and become saturated beyond this value. The optimum band gap that we obtain is the same as the previous works [1, 2].

From our two band model, we can explain the first-principles calculation results. The 2D PbTe has a low ZT value because it possesses flat bands near its band edge, while 2D SiGe has a low band gap resulting in a low ZT . On the other hand, Bi_2Te_3 and Bi_2Se_3 bands are corrugated near the Fermi level and are not classified as the flat band as described by the

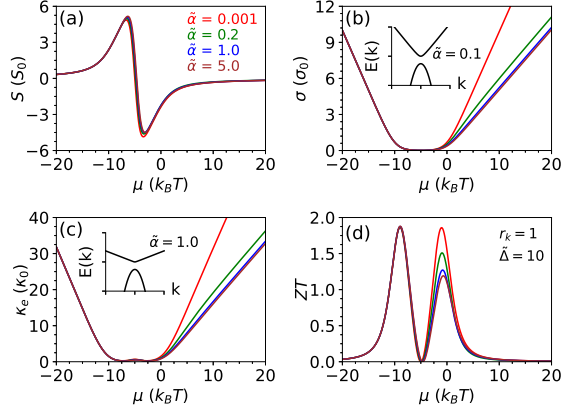


Fig. 5. (a) Seebeck coefficient, (b) electrical conductivity, (c) electronic thermal conductivity, and (d) ZT calculated from the 2D two-band model with $\tilde{\Delta} = 10 k_B T$ and several band flatness. The phonon thermal conductivity $\kappa_{ph} = \kappa_0 r_k$ is set to be κ_0 . The units are defined as follows, $S_0 = \frac{k_B}{q}$, $\sigma_0 = \frac{Cq^2}{2\pi\hbar^2}(k_B T)$, and $\kappa_0 = \frac{Ck_B^3 T^2}{4\pi\hbar^2}$. The inset gives the band dispersions on $\tilde{\alpha} = 0.1$ and $\tilde{\alpha} = 1.0$

Kane model, so the results from our model cannot be used to describe these materials. The Corrugated flat band has multiple Fermi pockets that, in effect, enhance the Seebeck coefficients [14]. We also note that in Fig. 3, there are a lot of sharp peaks in 2D Bi₂Te₃ and 2D Bi₂Se₃ DOS, while 2D SiGe and 2D PbTe have less of them.

Our continuum model is not able to explain the effect of narrow band width on TE properties. According to the previous works [30], the upper limit of ZT is achieved by having a transport distribution function (TDF) that resembles the Dirac delta function. However, according to [3, 31], such TDF cannot be achieved in the real material. Even if the DOS shows the Van Hove singularities, the TDF is not divergent because the DOS term is canceled out with the square of longitudinal velocity term resulting in a finite ZT [32]. The narrow transport distribution gives more conducting channels that increase

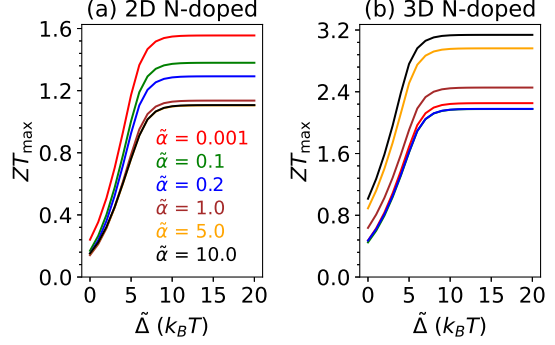


Fig. 6. ZT at optimal μ (ZT_{max}) vs band gap $\tilde{\Delta}$ for various band flatness. ZT_{max} increases proportionally with $\tilde{\Delta}$ up to around $10 k_B T$.

σ while giving a low κ_{el} because of the $(E - \mu)^2$ factor that κ_{el} has [3, 31]. Sharp peaks in DOS have also been found in previous works [33, 34], which enhance the Seebeck coefficient. These works explain why 2D Bi₂Te₃ and 2D Bi₂Se₃, which have corrugated bands plus sharp peaks in DOS, possess a high ZT .

The optimized chemical potential and its associated carrier concentration are given in Table. 4. After obtaining the optimized chemical potentials, we calculate the temperature-dependent relaxation time and phonon thermal conductivity on those chemical potentials. The relaxation times of each material on various temperatures are obtained using the same method to get the value in Table 1. As for the phonon conductivities, we obtain them directly from the experimental data fitting. All of the phonon conductivities exhibit a $1/T$ dependency. We then try to see if the fitted relaxation time can display a similar trend with the experimental data by comparing the electrical conductivities (Fig. 7 second row). It was shown that the temperature dependency we got from Fig. 9 represents the experimental data poorly. Therefore, we fit the relaxation time from the electrical conductivities directly by using the σ/\mathcal{T} value from the calculation at the optimized chemical potential, which gives better results. The discrepancies occur because experimental carrier concentrations were unknown. We then compare both

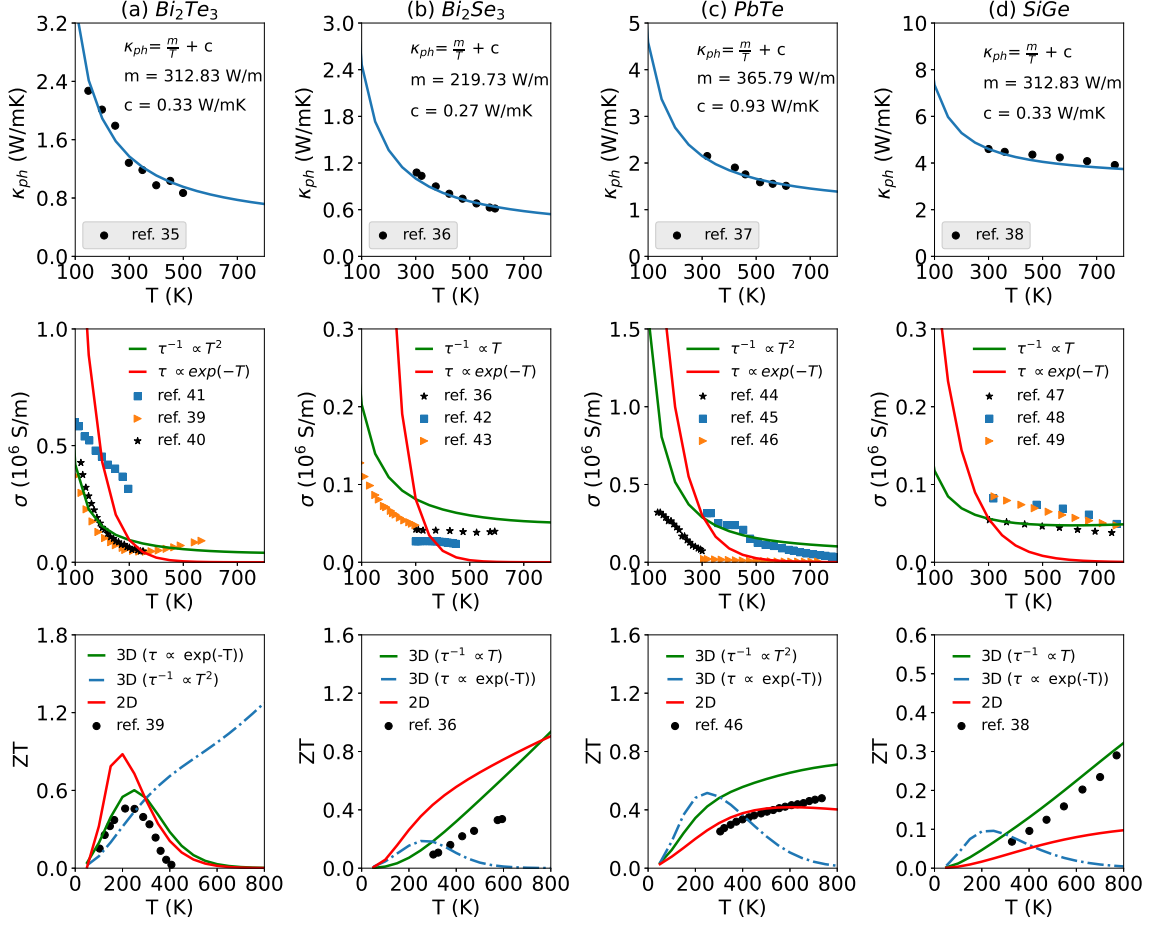


Fig. 7. Phonon thermal conductivity (first row) curve fitting for (a) Bi_2Te_3 [35], (b) Bi_2Se_3 [36], (c) PbTe [37], and (d) SiGe [38] as a function of temperature. The second row shows the results of the fitting from Fig. 9 in Appendix and direct fitting on electric conductivity. The temperature dependence of ZT values are shown in the third row, the green line indicates that the fittest relaxation time is used, while the red line indicates the 2D ZT value. All thermoelectric properties are calculated on its optimized chemical potential.

of relaxation time function in the ZT value (Fig. 7 third row).

From the plot, we can see that the exponential relaxation time capture the temperature dependency of Bi_2Te_3 data Ref. [39]. In Bi_2Se_3 and SiGe , the relaxation time is proportional to $1/T$, while in PbTe , it is proportional to $1/T^2$. The same temperature dependencies are used for each corresponding 2D material due to the limited experimental data. The fittest

relaxation time functions are as follow,

$$\begin{aligned}\tau_{\text{Bi}_2\text{Te}_3} &= 6.88 \exp(-T/54.5) \text{ ps}, \\ \tau_{\text{Bi}_2\text{Se}_3} &= 2.098 T^{-1} \text{ ps}, \\ \tau_{\text{PbTe}} &= 0.948 T^{-2} \text{ ns}, \\ \tau_{\text{SiGe}} &= 2.4 T^{-1} \text{ ps}.\end{aligned}$$

In room temperature, all of the relaxation times are in the order of fs.

The ZT value of a single QL Bi_2Te_3 is bigger on low temperature ($< 300\text{K}$), and the value drops beyond the room temperature like

its bulk counterpart. The single QL Bi_2Se_3 showcase a better ZT value on all temperature ranges except on $> 800\text{K}$. For PbTe and SiGe , we can see that the bulk ZT values are higher than 2D values on all temperature range. None of the materials reaches a ZT value much higher than unity, the highest 2D ZT value is achieved by Bi_2Te_3 in low temperature regime (around 0.88 at 200K) and Bi_2Se_3 in high temperature regime (around 0.9 at 800K). The highest bulk ZT value is achieved by Bi_2Se_3 on 800K (around 0.93).

In conclusion, we have calculated the thermoelectric properties of the bulk and the 2D structures of Bi_2Te_3 , Bi_2Se_3 , PbTe , and SiGe . We used temperature-dependent relaxation time approximation to obtain the transport properties. The single QL of Bi_2Te_3 and Bi_2Se_3 exhibits a higher ZT than its bulk due to their corrugated flat band, which agree with HD theory. However, PbTe and SiGe violate the HD theory. From the two-band model analysis, 2D PbTe and SiGe have lower ZT than 3D counterparts because 2D PbTe has flat bands and 2D SiGe has a low band gap. We note that these low ZT occur even when the DOS of 2D materials are higher than 3D. The fact that HD theory is non-universal requires a deeper analysis of which material or geometry performs the best at a given dimension.

The figure of merits on all materials, except Bi_2Te_3 , increase as the temperature increases. The single QL of Bi_2Te_3 has a higher ZT value below room temperature, while the single QL of Bi_2Se_3 has a higher ZT value on temperature range below 800K . PbTe and SiGe monolayers have lower ZT values on all temperature ranges than their bulk. Better results might be achieved when one can manipulate the relaxation mechanisms to reduce phonon thermal conductivity and to increase electrical conductivity for the bulk and the 2D structures.

Acknowledgments

The computation in this work has been done using the facilities of HPC LIPI, Indonesian Institute of Sciences (LIPI). EHH acknowledges ATTRACT 7556175 and CORE 11352881

References

- [1] Hasdeo E H, Krisna L P, Hanna M Y, Gunara B E, Hung N T and Nugraha A R 2019 *Journal of Applied Physics* **126** 1–10
- [2] Sofo J O and Mahan G D 1994 *Phys. Rev. B* **49**(7) 4565–4570
- [3] Zhou J, Yang R, Chen G and Dresselhaus M S 2011 *Phys. Rev. Lett.* **107**(22) 226601
- [4] Hicks L D and Dresselhaus M S 1993 *Phys. Rev. B* **47**(19) 12727–12731
- [5] Hicks L D and Dresselhaus M S 1993 *Phys. Rev. B* **47**(24) 16631–16634
- [6] Biswas K, He J, Blum I D, Wu C I, Hogan T P, Seidman D N, Dravid V P and Kanatzidis M G 2012 *Nature* **489** 414–418
- [7] Hochbaum A I, Chen R, Delgado R D, Liang W, Garnett E C, Najarian M, Majumdar A and Yang P 2008 *Nature* **451** 163–167
- [8] Poudel B, Hao Q, Ma Y, Lan Y, Minnich A, Yu B, Yan X, Wang D, Muto A, Vashaee D, Chen X, Liu J, Dresselhaus M S, Chen G and Ren Z 2008 *Science* **320** 634–638
- [9] Hung N T, Hasdeo E H, Nugraha A R, Dresselhaus M S and Saito R 2016 *Physical Review Letters* **117** 1–5
- [10] Teweldebrhan D, Goyal V and Balandin A A 2010 *Nano Letters* **10** 1209–1218
- [11] Sun Y, Cheng H, Gao S, Liu Q, Sun Z, Xiao C, Wu C, Wei S and Xie Y 2012 *Journal of the American Chemical Society* **134** 20294–20297
- [12] Liu J, Qian X and Fu L 2015 *Nano Letters* **15** 2657–2661
- [13] Jamdagni P, Kumar A, Thakur A, Pandey R and Ahluwalia P K 2015 *Materials Research Express* **2** 16301
- [14] Mori K, Usui H, Sakakibara H, Kuroki K, Mori K, Usui H and Sakakibara H 2016 **042108**
- [15] Giannozzi P, Baroni S, Bonini N, Calandra M, Car R, Cavazzoni C, Ceresoli D, Chiarotti G L, Cococcioni M, Dabo I, Corso A D, de Gironcoli S, Fabris S, Fratesi G, Gebauer R, Gerstmann U, Gougoussis C, Kokalj A, Lazzeri M, Martin-Samos L, Marzari N, Mauri F, Mazzarello R, Paolini S, Pasquarello A, Paulatto L, Sbraccia C, Scandolo S, Sclauzero G, Seitsonen A P, Smogunov A, Umari P and Wentzcovitch R M 2009 *Journal of Physics: Condensed Matter* **21** 395502

- [16] Kresse G and Joubert D 1999 *Phys. Rev. B* **59**(3) 1758–1775
- [17] Perdew J P, Chevary J A, Vosko S H, Jackson K A, Pederson M R, Singh D J and Fiolhais C 1992 *Phys. Rev. B* **46**(11) 6671–6687
- [18] Monkhorst H J and Pack J D 1976 *Phys. Rev. B* **13**(12) 5188–5192
- [19] Madsen G K and Singh D J 2006 *Computer Physics Communications* **175** 67–71
- [20] **Supplementary material** link is provided by the publisher
- [21] Jia Y Z, Ji W X, Zhang C W, Li P, Zhang S F, Wang P J, Li S S and Yan S S 2017 *Physical Chemistry Chemical Physics* **19** 29647–29652
- [22] Sannyl A, Ahn Y and Jang J 2019 *Computational Materials Science* **165** 121–128
- [23] Witting I T, Chasapis T C, Ricci F, Peters M, Heinz N A, Hautier G and Snyder G J 2019 *Advanced Electronic Materials* **5** 1–20
- [24] Zhou G and Wang D 2015 *Scientific Reports* **5** 1–6
- [25] Ryu B and Oh M W 2016 *Journal of the Korean Ceramic Society* **53** 273–281
- [26] Park S and Ryu B 2016 *Journal of the Korean Physical Society* **69** 1683–1687
- [27] Wang Y, Chen X, Cui T, Niu Y, Wang Y, Wang M, Ma Y and Zou G 2007 *Physical Review B - Condensed Matter and Materials Physics* **76** 1–10
- [28] Zhao Z Y, Yang W and Yang P Z 2016 *Chinese Physics B* **25**
- [29] Markov M, Rezaei S E, Sadeghi S N, Esfarjani K and Zebarjadi M 2019 *Physical Review Materials* **3** 1–7
- [30] Mahan G D and Sofo J O 1996 *Proceedings of the National Academy of Sciences* **93** 7436–7439
- [31] Jeong C, Kim R and Lundstrom M S 2012 *Journal of Applied Physics* **111** 0–12
- [32] Nurhuda M, Nugraha A R T, Hanna M Y, Suprayoga E and Hasdeo E H 2020 *Advances in Natural Sciences: Nanoscience and Nanotechnology* **11** 015012
- [33] Mi X Y, Yu X, Yao K L, Huang X, Yang N and LÄCE J T 2015 *Nano Letters* **15** 5229–5234
- [34] Ding Z, An M, Mo S, Yu X, Jin Z, Liao Y, Esfarjani K, LÄCE J T, Shiomi J and Yang N 2019 *J. Mater. Chem. A* **7**(5) 2114–2121
- [35] Qiu B and Ruan X 2010 *Applied Physics Letters* **97** 2–4
- [36] Liu R, Tan X, Ren G, Liu Y, Zhou Z, Liu C, Lin Y and Nan C 2017 *Crystals* **7**
- [37] Orihashi M, Noda Y, Chen L and Hirai T 2000 *Materials Transactions, JIM* **41** 1196–1201
- [38] Tayebi L, Zamanipour Z, Mozafari M, Norouzzadeh P, Krasinski J S, Ede K F and Vashaee D 2012 Thermal and thermoelectric properties of nanostructured versus crystalline sige *IEEE Green Technologies Conference* (Tulsa, OK, USA) p 1–4
- [39] Jeon H W, Ha H P, Hyun D B and Shim J D 1991 *Journal of Physics and Chemistry of Solids* **52** 579–585
- [40] Plecháček T, Navrátil J, Horák J and Lošťák P 2004 *Philosophical Magazine* **84** 2217–2228
- [41] Kulbachinskii V A, Kytin V G, Kudryashov A A and Tarasov P M 2012 *Journal of Solid State Chemistry* **193** 47–52
- [42] Hong M, Chen Z G, Yang L, Han G and Zou J 2015 *Advanced Electronic Materials* **1** 1–9
- [43] Hor Y S, Richardella A, Roushan P, Xia Y, Checkelsky J G, Yazdani A, Hasan M Z, Ong N P and Cava R J 2009 *Physical Review B - Condensed Matter and Materials Physics* **79** 2–6
- [44] McGuire M A, Malik A S and DiSalvo F J 2008 *Journal of Alloys and Compounds* **460** 8–12
- [45] Basu R, Bhattacharya S, Bhatt R, Singh A, Aswal D K and Gupta S K 2013 *Journal of Electronic Materials* **42** 2292–2296
- [46] Pei Y L and Liu Y 2012 *Journal of Alloys and Compounds* **514** 40–44
- [47] Nozariasbmarz A, Roy P, Zamanipour Z, Dycus J H, Cabral M J, LeBeau J M, Krasinski J S and Vashaee D 2016 *APL Materials* **4**
- [48] Wang X W, Lee H, Lan Y C, Zhu G H, Joshi G, Wang D Z, Yang J, Muto A J, Tang M Y, Klatsky J, Song S, Dresselhaus M S, Chen G and Ren Z F 2008 *Applied Physics Letters* **93** 21–24
- [49] Bathula S, Jayasimhadri M, Singh N, Srivastava A K, Pulikkotil J, Dhar A and Budhani R C 2012 *Applied Physics Letters* **101**
- [50] Janiček, P. and Drašar, Č. and Beneš, L. and Lošťák, P 2009 *Crystal Research and Technology* **44** 505–510
- [51] Scheidemantel J, Ambrosch-Draxl C, Thonhauser T, Badding V and Sofo O 2003 *Physical Review B - Condensed Matter and Materials Physics* **68** 1–6
- [52] Goldsmid H J, Sheard A R and Wright D A 1958 *British Journal of Applied Physics* **9** 365–370
- [53] Hunter J D 2007 *Computing in Science & Engineering* **9** 90–95
- [54] Nakajima S 1963 *Journal of Physics and Chemistry of Solids* **24** 479–485
- [55] Huang B L and Kaviani M 2008 *Physical Review B - Condensed Matter and Materials Physics* **77** 1–19
- [56] Dalven R 1969 *Infrared Physics* **9** 141–184
- [57] Sharma S and Schwingenschlöggl U 2016 *ACS Energy Letters* **1** 875–879
- [58] Steele M C and Rosi F D 1958 *Journal of Applied Physics* **29** 1517–1520

Supplementary Material

Appendix A: Relaxation Time Fitting

Here we present the fitting method to obtain the relaxation time at various temperatures. The method is adopted from Scheidemantel's and Goldsmid's work [51, 52]. All the fitting results are shown in Fig. 8. We plot the Seebeck coefficient with respect to the electrical conductivity on each chemical potential at a certain temperature from BoltzTraP outputs. The electrical conductivity from BoltzTraP is in the form of S/\mathcal{T} , thus we can compare the plot with experimental data to obtain the relaxation time on a certain temperature.

From the fitting results in Fig. 8, we can do an additional curve fitting to obtain the temperature dependency (Fig. 9). It is shown that all of the material has an exponential dependency on the temperature. But it is shown in Fig. 7, that they describe the conductivity poorly. So we tried to do a direct curve fitting with the conductivity to obtain a better relaxation time. Experiment data from [40, 43, 45, 47] are used for the direct curve fitting of Bi_2Te_3 , Bi_2Se_3 , PbTe , and SiGe , respectively. We fixed the relaxation time on 300 K to the values in Table. 1 on the direct curve fitting to attain the same thermoelectric properties we have calculated on Fig. 4.

Appendix B: Asymmetric Bands

Here we present the formulation we used to calculate the thermoelectric properties of asymmetric bands. We used two-bands model, with parabolic band as the valence band and Kane band as the conduction band, both are defined as,

$$E_{Kane}^{cb} = \sqrt{\frac{\hbar^2 k^2}{2m\alpha} + \frac{1}{4\alpha^2}} - \frac{1}{2\alpha}, \quad (2)$$

$$E_{parabolic}^{vb} = -\frac{\hbar^2 k^2}{2m} - \Delta, \quad (3)$$

where Δ is the band gap and α is the non-parabolicity factor. The value of $\alpha = 0$ corresponds to a parabolic band. The transport properties from Boltzmann's transport theory under relaxation time approximation (RTA), for each band, are given by,

$$\sigma = q^2 \mathcal{L}_0, \quad (4)$$

$$S = \frac{1}{qT} \frac{\mathcal{L}_1}{\mathcal{L}_0}, \quad (5)$$

$$\kappa_e = \frac{1}{T} \left(\mathcal{L}_2 - \frac{(\mathcal{L}_1)^2}{\mathcal{L}_0} \right), \quad (6)$$

$$ZT = \frac{\sigma S^2}{\kappa_e + \kappa_{ph}} T, \quad (7)$$

where \mathcal{L}_i is the TE integral and is defined as,

$$\mathcal{L}_{i,vb} = \int_{-\infty}^0 \tau(E) (E - \mu)^i \left(-\frac{\partial f}{\partial E} \right) dE, \quad (8)$$

$$\mathcal{L}_{i,cb} = \int_0^{\infty} \tau(E) (E - \mu)^i \left(-\frac{\partial f}{\partial E} \right) dE, \quad (9)$$

where μ is the Fermi energy, $f(E)$ is the Fermi-Dirac distribution, and $\mathcal{T}(E)$ is the transport distribution function (TDF). The explicit form of TDF with constant relaxation time approximation (CRTA) is $\mathcal{T}(E) = v_x^2(E)\tau(E)D(E)$ and has a different form on each band dispersion and dimension. The TDF that are used in the calculations are:

$$\mathcal{T}(E)_{\text{kane}}^{2D} = C \left(\frac{1}{4m\alpha} \right) \frac{E(E + \frac{1}{\alpha})}{(E + \frac{1}{2\alpha})^2} D(E)_{\text{kane}}^{2D}, \quad (10)$$

$$\mathcal{T}(E)_{\text{kane}}^{3D} = C \left(\frac{1}{6m\alpha} \right) \frac{E(E + \frac{1}{\alpha})}{(E + \frac{1}{2\alpha})^2} D(E)_{\text{kane}}^{3D}, \quad (11)$$

$$\mathcal{T}(E)_{\text{parabolic}}^{2D} = C \left(\frac{-E - \Delta}{m} \right) D_{\text{parabolic}}^{2D}, \quad (12)$$

$$\mathcal{T}(E)_{\text{parabolic}}^{3D} = C \left(\frac{-E - \Delta}{m} \right) D_{\text{parabolic}}^{3D}. \quad (13)$$

The DOS of each band dispersions and dimensions can be written as,

$$D(E)_{\text{kane}}^{2D} = \frac{m\alpha}{\pi\hbar^2} \left(E + \frac{1}{2\alpha} \right), \quad (14)$$

$$D(E)_{\text{kane}}^{3D} = \frac{1}{2\pi^2} \left(\frac{2m\alpha}{\hbar^2} \right)^{3/2} \left(E + \frac{1}{2\alpha} \right) \left(E \left(E + \frac{1}{\alpha} \right) \right)^{1/2}, \quad (15)$$

$$D(E)_{\text{parabolic}}^{2D} = \frac{m}{2\pi\hbar^2} \Theta(|E| - |\Delta|), \quad (16)$$

$$D(E)_{\text{parabolic}}^{3D} = \frac{\sqrt{2}m^{3/2}}{2\pi^2\hbar^3} (-E - \Delta)^{1/2} \Theta(|E| - |\Delta|), \quad (17)$$

where Θ is the Heaviside function. Defining the dimensionless quantity as

$$\begin{aligned} E &= \epsilon k_B T, \\ \mu &= \eta k_B, \\ \Delta &= \tilde{\Delta} k_B T, \\ \alpha &= \frac{\tilde{\alpha}}{k_B T}, \end{aligned}$$

plus letting $x = \epsilon - \eta$, the TE integral then become:

$$\mathcal{L}_{i,c}^{2D} = \frac{C}{4\pi\hbar^2} (k_B T)^{i+1} \mathcal{H}_{i,c}(\eta), \quad (18)$$

$$\mathcal{L}_{i,v}^{2D} = \frac{C}{2\pi\hbar^2} (k_B T)^{i+1} \left[\mathcal{F}_{i+1,v}(\eta + \tilde{\Delta}) + (\eta + \tilde{\Delta}) \mathcal{F}_{i,v}(\eta + \tilde{\Delta}) \right], \quad (19)$$

$$\mathcal{L}_{i,c}^{3D} = \frac{C(2m)^{1/2}}{6\pi^2\hbar^3} (k_B T)^{i+3/2} \mathcal{I}_{i,c}(\eta), \quad (20)$$

$$\mathcal{L}_{i,v}^{3D} = \frac{C(2m)^{1/2}}{3\pi^2\hbar^3} (k_B T)^{i+3/2} \mathcal{J}_{i,v}(\eta + \tilde{\Delta}), \quad (21)$$

where $\mathcal{H}_{i,c}(\eta)$, $\mathcal{F}_{i,v}(\eta)$, $\mathcal{I}_{i,c}(\eta)$, $\mathcal{J}_{i,v}(\eta)$ are defined as:

$$\mathcal{H}_{i,c}(\eta) = \int_{-\eta}^{\infty} x^i \frac{(x+\eta)(x+\eta+1/\tilde{\alpha})}{(x+\eta+1/2\tilde{\alpha})} \frac{\exp(x)}{(\exp(x)+1)^2} dx, \quad (22)$$

$$\mathcal{F}_{i,v}(\eta) = - \int_{-\infty}^{-\eta} x^i \frac{\exp(x)}{(\exp(x)+1)^2} dx, \quad (23)$$

$$\mathcal{I}_{i,c}(\eta) = \tilde{\alpha}^{1/2} \int_{-\eta}^{\infty} x^i \left[\frac{(x+\eta)^3(x+\eta+1/\tilde{\alpha})^3}{(x+\eta+1/2\tilde{\alpha})^2} \right]^{1/2} \frac{\exp(x)}{(\exp(x)+1)^2} dx, \quad (24)$$

$$\mathcal{J}_{i,v}(\eta) = \int_{-\infty}^{-\eta} x^i (-x-\eta-\tilde{\Delta})^{3/2} \frac{\exp(x)}{(\exp(x)+1)^2} dx. \quad (25)$$

Only $\mathcal{F}_{i,v}(\eta)$ can be solved analytically out of the four integrals. The analytic results for these integrals are:

$$\mathcal{F}_{0,v}(\eta) = \frac{1}{e^\eta + 1}, \quad (26)$$

$$\mathcal{F}_{1,v}(\eta) = -\frac{\eta}{e^\eta + 1} - \ln(1 + e^{-\eta}), \quad (27)$$

$$\mathcal{F}_{2,v}(\eta) = \frac{\eta^2}{e^\eta + 1} + 2\eta \ln(1 + e^{-\eta}) - 2\text{Li}_2(-e^{-\eta}), \quad (28)$$

$$\mathcal{F}_{3,v}(\eta) = \eta^2 \left(\frac{\eta}{1 + e^\eta} + 3 \ln(1 + e^{-\eta}) \right) - 6\eta \text{Li}_2(-e^{-\eta}) - 6\text{Li}_3(-e^{-\eta}) \quad (29)$$

with $\text{Li}_k(z) = \sum_{n=1}^{\infty} \frac{z^n}{n^k}$.

We can obtain thermoelectric properties by plugging eq. (18) - (21) to eq. (4) - (6). The transports from conduction band have the form of:

$$\sigma_c^{2d} = \frac{Cq^2}{4\pi\hbar^2} (k_B T) \mathcal{H}_{0,c}(\eta) = \sigma_c^{2d} = \sigma_c^0 \tilde{\sigma}_c^{2d} \implies \sigma_c^0 = \frac{Cq^2}{4\pi\hbar^2} (k_B T), \quad (30)$$

$$S_c^{2d} = -\frac{k_B}{q} \frac{\mathcal{H}_{1,c}(\eta)}{\mathcal{H}_{0,c}(\eta)} = -S_c^0 \tilde{S}_c^0 \implies S_c^0 = \frac{k_B}{q}, \quad (31)$$

$$\kappa_{e,c}^{2d} = \frac{Ck_B^3 T^2}{4\pi\hbar^2} \left(\mathcal{H}_{2,c} - \frac{(\mathcal{H}_{1,c})^2}{\mathcal{H}_{0,c}} \right) = \kappa_{e,c}^0 \tilde{\kappa}_{e,c}^0 \implies \kappa_{e,c}^0 = \frac{Ck_B^3 T^2}{4\pi\hbar^2}, \quad (32)$$

while the transports from the valence have the form of:

$$\begin{aligned} \sigma_v^{2d} &= \frac{Cq^2}{2\pi\hbar^2} (k_B T) \left[\mathcal{F}_{1,v}(\eta + \tilde{\Delta}) + (\eta + \tilde{\Delta}) \mathcal{F}_{0,v}(\eta + \tilde{\Delta}) \right] \\ &= \sigma_v^0 \tilde{\sigma}_v^{2d} \implies \sigma_v^0 = \frac{Cq^2}{2\pi\hbar^2} (k_B T), \end{aligned} \quad (33)$$

$$\begin{aligned} S_v^{2d} &= -\frac{k_B}{q} \left[\frac{\mathcal{F}_{2,v}(\eta + \tilde{\Delta}) + (\eta + \tilde{\Delta}) \mathcal{F}_{1,v}(\eta + \tilde{\Delta})}{\mathcal{F}_{1,v}(\eta + \tilde{\Delta}) + (\eta + \tilde{\Delta}) \mathcal{F}_{0,v}(\eta + \tilde{\Delta})} \right] \\ &= -S_v^0 \tilde{S}_v^0 \implies S_v^0 = \frac{k_B}{q}, \end{aligned} \quad (34)$$

$$\begin{aligned}
\kappa_{e,v}^{2d} &= \frac{Ck_B^3 T^2}{4\pi\hbar^2} \left(\mathcal{H}_{2,c} - \frac{(\mathcal{H}_{1,c})^2}{\mathcal{H}_{0,c}} \right) \\
&= \frac{Ck_B^3 T^2}{4\pi\hbar^2} \left[\left(\mathcal{F}_{3,v}(\eta + \tilde{\Delta}) + (\eta + \tilde{\Delta})\mathcal{F}_{2,v}(\eta + \tilde{\Delta}) \right) \right. \\
&\quad \left. - \left(\frac{\mathcal{F}_{2,v}(\eta + \tilde{\Delta}) + (\eta + \tilde{\Delta})\mathcal{F}_{1,v}(\eta + \tilde{\Delta})}{\mathcal{F}_{1,v}(\eta + \tilde{\Delta}) + (\eta + \tilde{\Delta})\mathcal{F}_{0,v}(\eta + \tilde{\Delta})} \right) \right] \\
&= \kappa_{e,v}^0 \tilde{\kappa}_{e,v}^0 \implies \kappa_{e,v}^0 = \frac{Ck_B^3 T^2}{4\pi\hbar^2}.
\end{aligned} \tag{35}$$

Looking at the transport quantities from eq. (30) - (35), the relations between the conduction band and the valence band are

$$\begin{aligned}
\sigma_c^0 &= \frac{1}{2}\sigma_v^0, \\
S_c^0 &= S_v^0, \\
\kappa_{e,c}^0 &= \frac{1}{2}\kappa_{e,v}^0.
\end{aligned}$$

The 3D formulation retains the same relation as above, and the transports equations are the same as the 2D formulation, differing only in the transport magnitude:

$$\begin{aligned}
\sigma_{c,3D}^0 &= \frac{Cq^2(2m)^{1/2}}{6\pi\hbar^2} (k_B T)^{3/2} \\
S_{c,3D}^0 &= \frac{k_B}{q} \\
\kappa_{e,c,3D}^0 &= \frac{C(2m)^{1/2}}{6\pi^2\hbar^3} k_B^{7/2} T^{5/2}
\end{aligned}$$

For the two-band model, the total transport properties are:

$$\begin{aligned}
\sigma &= \sigma^c + \sigma^v \\
&= \sigma_v^0 \left(\frac{1}{2}\tilde{\sigma}_c^0 + \tilde{\sigma}_v^0 \right) \\
&= \sigma_v^0 \tilde{\sigma}.
\end{aligned} \tag{36}$$

$$\begin{aligned}
S &= \frac{\sigma^c S^c + \sigma^v S^v}{\sigma^c + \sigma^v} \\
&= S_v^0 \left[\frac{\frac{1}{2}\tilde{\sigma}_c^0 \tilde{S}_c^0 + \tilde{\sigma}_v^0 \tilde{S}_v^0}{\frac{1}{2}\tilde{\sigma}_c^0 + \tilde{\sigma}_v^0} \right] \\
&= S_v^0 \tilde{S}.
\end{aligned} \tag{37}$$

$$\begin{aligned}
\kappa_e &= \frac{\sigma^c \sigma^v}{\sigma^c + \sigma^v} (S^c - S^v)^2 + (\kappa_e^c + \kappa_e^v) \\
&= \kappa_{e,v}^0 \left[\frac{\frac{1}{2} \tilde{\sigma}_c^0 \tilde{\sigma}_v^0}{\frac{1}{2} \tilde{\sigma}_c^0 + \tilde{\sigma}_v^0} (\tilde{S}_c^0 - \tilde{S}_v^0)^2 + \left(\frac{1}{2} \tilde{\kappa}_{e,0}^c + \tilde{\kappa}_{e,0}^v \right) \right] \\
&= \kappa_{e,v}^0 \tilde{\kappa}_e.
\end{aligned} \tag{38}$$

$$\begin{aligned}
ZT &= \frac{\sigma S^2}{\kappa_e + \kappa_{ph}} \\
&= \frac{\tilde{\sigma} \tilde{S}^2}{\tilde{\kappa}_e + r_k}.
\end{aligned} \tag{39}$$

Phonon thermal conductivity is defined as $\kappa_{ph} = r_k \kappa_{e,v}^0$ in the equations above. We use $r_k = 1$ in all our calculations.

Each transport properties from multiple bands can be written as the summation of the kernel integrals, with n as the total number of bands,

$$\sigma = q^2 \sum_{i=1}^n \mathcal{L}_{0,i} = \sum_{i=1}^n \sigma_i, \tag{40}$$

$$S = \frac{1}{qT} \frac{\sum_{i=1}^n \mathcal{L}_{1,i}}{\sum_{i=1}^n \mathcal{L}_{0,i}} = \frac{\sum_{i=1}^n S_i \sigma_i}{\sum_{i=1}^n \sigma_i} \tag{41}$$

$$\begin{aligned}
\kappa_e &= \frac{1}{T} \left(\sum_{i=1}^n \mathcal{L}_{2,i} - \frac{(\sum_{i=1}^n \mathcal{L}_{1,i})^2}{\sum_{i=1}^n \mathcal{L}_{0,i}} \right) \\
&= \sum_{i=1}^n \kappa_{e,i} + \sum_{\substack{i,j \\ i \neq j}}^n \frac{\sigma_i \sigma_j}{\sigma_i + \sigma_j} (S_i - S_j)^2
\end{aligned} \tag{42}$$

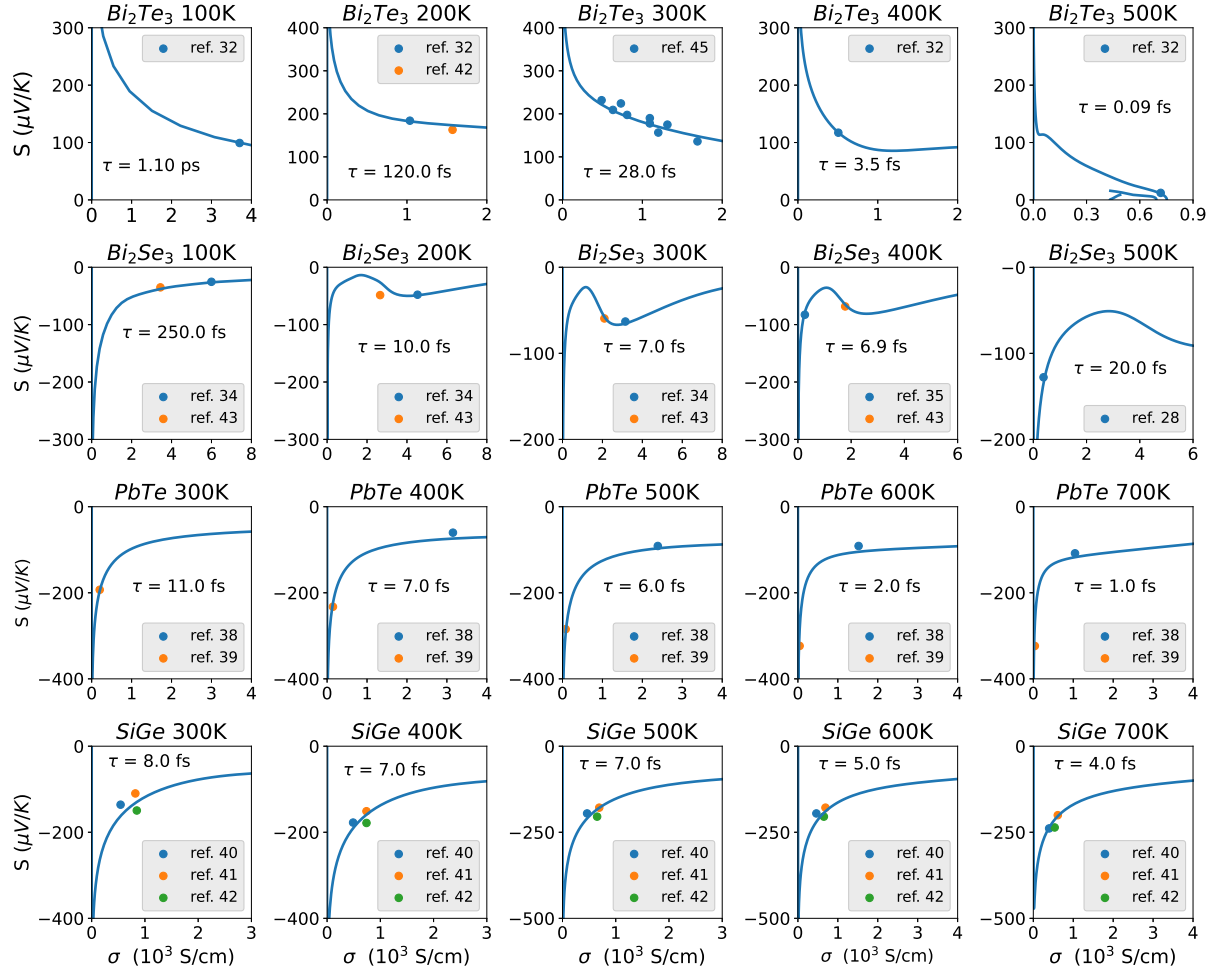


Fig. 8. Comparison of Seebeck coefficient versus electrical conductivity from the BoltzTraP outputs and experimental data to obtain the relaxation time at various temperature.

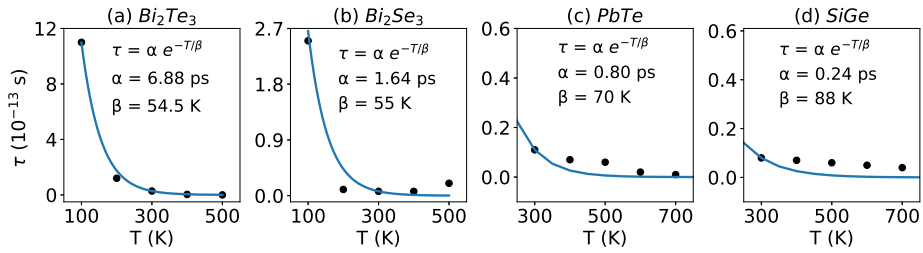


Fig. 9. Temperature dependency of the relaxation time obtained from curve fitting. Each data is the result of the curve fitting in Fig. 8

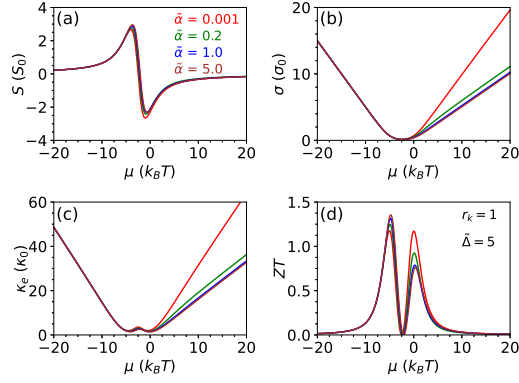


Fig. 10. Thermoelectric properties of 2D two-bands model on several band flatness with $\tilde{\Delta} = 5$ and $r_k = 1$.

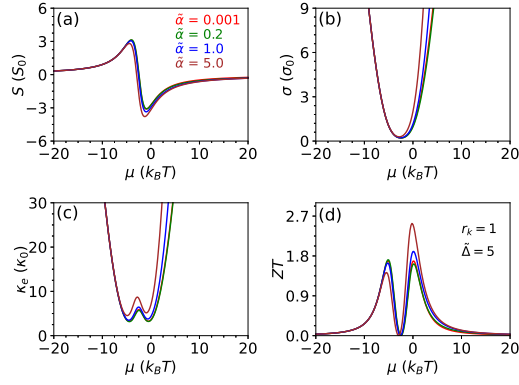


Fig. 11. Thermoelectric properties of 3D two-bands model on several band flatness with $\tilde{\Delta} = 5$ and $r_k = 1$.

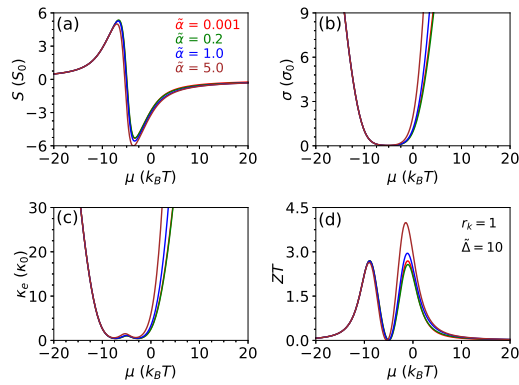


Fig. 12. Thermoelectric properties of 3D two-bands model on several band flatness with $\tilde{\Delta} = 10$ and $r_k = 1$.

Table. 3. Relaxed lattice constants

	$a = b$ (Å)	Experiment (Å)	Computation (Å)
3D Material			
Bi ₂ Te ₃	10.6555	10.476 [47]	10.473 [48]
Bi ₂ Se ₃	10.012	9.84 [47]	-
PbTe	6.5337	6.464 [49]	-
SiGe	5.5916	5.527 [51]	5.5955 [26]
2D Material			
Bi ₂ Te ₃	4.4162	-	4.38 [50]
Bi ₂ Se ₃	4.1653	4.13 [11]	-
PbTe	6.5321	-	-
SiGe	3.9549	-	3.91 [20]

Table. 4. Optimized chemical potentials and their corresponding carrier concentrations and ZT values

	Maximum ZT	μ_{opt} (eV)	n (10^{19} cm^{-3})
3D Material			
Bi ₂ Te ₃	0.54	-0.084	2.02 (p)
Bi ₂ Se ₃	0.18	-0.208	17.6 (p)
PbTe	0.49	-0.131	20.1 (p)
SiGe	0.09	0.648	9.40 (n)
2D Material			
Bi ₂ Te ₃	0.57	0.016	2.74 (n)
Bi ₂ Se ₃	0.43	0.039	2.40 (n)
PbTe	0.32	0.121	9.40 (p)
SiGe	0.04	-0.066	3.25 (p)